

Threshold Curve for the Excitability of Bidimensional Spiking Neurons

Arnaud Tonnelier

INRIA-Grenoble 655 avenue de l'Europe, Montbonnot

38334 Saint Ismier, France *

(Dated: July 29, 2014)

We shed light on the threshold for spike initiation in two-dimensional neuron models. A threshold criterion that depends on both the membrane voltage and the recovery variable is proposed. This approach provides a simple and unified framework that accounts for numerous voltage threshold properties including adaptation, variability and time-dependent dynamics. In addition, neural features such as accommodation, inhibition-induced spike, and post-inhibitory (-excitatory) facilitation are the direct consequences of the existence of a threshold curve. Implications for neural modeling are also discussed.

I. INTRODUCTION

The dynamics of spiking neurons is characterized by two distinct regimes monitored by the membrane potential, v , of the neuron: at moderate v values, typically lower than $-55mV$, the neuron acts as a linear filter, while for greater values of the membrane voltage ($> -40mV$) the dynamics is highly nonlinear and follows a stereotyped trajectory, almost independent of the input, that represents an action potential or spike. At intermediate values, the neuron may switch in both regimes, depending on its internal state and the input. This feature defines the so-called neural excitability [1, 2] and relies on the existence of a threshold effect that is explicitly described in simple spiking neural models of integrate-and-fire type by a strict voltage threshold of the form $v = \theta$ where θ is a given voltage value, i.e., the intermediate regime, $-55mV < v < -40mV$, is reduced to a threshold line separating a subthreshold region from a super-threshold region.

In contrast with standard integrate-and-fire neurons, detailed biophysical models of the Hodgkin-Huxley type do not have an explicit firing threshold and due to the continuous nature of the underlying differential system, there is a continuum of trajectories, from sharp action potential to small depolarization, making the concept of threshold ambiguous. However, it has been shown that the switching to the super-threshold regime occurs in a narrow range of input values, and a *quasi-threshold* [3] effect is observed. This effect is commonly approximated by a strict voltage threshold [4, 5]. The partition of the phase space between a subthreshold region and a super-threshold region is closely related to the separation of time-scales between a fast action potential, with a time scale of order $1ms$, and a slower subthreshold dynamics of input integration, of order greater than $10ms$. When the fast dynamics is assumed to be instantaneous, the spike description is ignored, and the super-threshold dynamics is reduced to an instantaneous reset, making the concept of threshold central in neural modeling as a synthesis of all nonlinear effects.

Several drawbacks are associated with using a clear-cut voltage threshold. Properties such as threshold variability or threshold dependence upon the spiking activity can not be adequately described. To overcome these limitations, time-dependent voltage thresholds have been introduced as an ad-hoc description of threshold fluctuations but lack rigorous derivation [6]. Recently, a voltage threshold equation has been derived from a quasi-static approximation of a Hodgkin-Huxley type model [7], and a series of work has revisited the concept of threshold manifolds in neural models [8–10]. Other threshold descriptions, including stochastic threshold models, have been introduced recently [11–15].

In this paper, we explore the threshold effect in bidimensional neural models and show that the strict voltage threshold $v = \theta$ [16] provides a poor approximation of the neural excitability whereas a threshold curve of the form $g(v) = u$, where u is a recovery (or adaptation) variable and g a non-monotonic function, accurately captures voltage threshold properties. Consequences for neural dynamics and neural modeling are discussed.

II. A THRESHOLD CURVE FOR BIDIMENSIONAL NEURAL MODELS

Sharp threshold models of neural firing offer an appealing framework to describe the neural activity and to analyze the neural dynamics. However, it has been long observed that the firing threshold is not a fixed number but rather a manifold [3, 17]. Two well-known situations clearly illustrate the existence of a threshold manifold that partitions the phase space into two regions. (i) In type I neural models, where the stable resting state coexists with a saddle node, the stable manifold of the saddle point, called the threshold separatrix, is identified as the locus of threshold phenomena [3, 17, 18]. (ii) In singularly perturbed systems, the firing threshold can be fairly well approximated by the middle branch of the N -shaped v -nullcline [17]. In addition, a close link has been recently established between the neural excitability and the existence of canard trajectories [8, 9], emphasizing the crucial role of the middle branch of the v -nullcline together with the existence of multiple time scales.

* arnaud.tonnelier@inria.fr

Here, we explore the concept of threshold in some popular neural models. For clarity and simplicity, we mainly consider bidimensional (2D) neural models where the time-dependent activity of the neuron is described by the membrane potential, $v(t)$, and an additional variable, $u(t)$, that accounts for adaptation, recovery processes, or, more generally, voltage-gated channels dynamics (sodium channel inactivation or potassium activation). Most often, the variable u acts as a negative feedback on v .

A well established stimulation paradigm for excitability-threshold extraction uses an instantaneous voltage change, i.e., a pulse of zero duration is applied to the membrane potential equation. For membrane potential above a critical voltage value, a spike is elicited and the recorded value defines the fast-depolarization threshold that may be obtained *in-vitro* using a short current pulse. This differs from the slow-depolarization threshold even though a close link exists between both thresholds [7]. In both cases, the recorded voltage threshold depends on the state of the neuron at the time of the stimulation, and we generalize the threshold-extraction method using an instantaneous shock of all variables. Taking a point in the phase space as an initial condition, we determine if a spike is elicited or not. More precisely, we compute the peak value of the membrane voltage, and a gray-level is assigned to the result: black regions indicate a spike and white stands for a small subthreshold response. Intermediate gray levels are used for intermediate responses. An arbitrary long time horizon is used to detect the peak value of the membrane voltage but, in practice, a maximum is reached in finite time, corresponding to the so-called spike-latency. The response surface of a linear system would be a grayscale gradient, i.e., with a clear distinction of all the intermediate responses, whereas an idealized on-off neuron model would lead to a binary black-and-white picture. The response surfaces of the bidimensional Abbott-Kepler reduction [19, 20], the Krinsky-Kokoz reduction [1, 21], the FitzHugh-Nagumo model [22, 23], the Morris-Lecar model [24], the adaptive quadratic integrate-and-fire (QIF) model (Izhikevich model [25]) and the adaptive exponential integrate-and-fire (EIF) model [26, 27] are plotted in Fig.1. Some characteristic elements are also displayed: the nullclines and the stable manifold of the saddle fixed point, when it exists.

The plots clearly show the existence, in the phase plane, of a tiny region where the peak value of the membrane potential blows up, delimiting a subthreshold region from a super-threshold region. This boundary defines a curve which is poorly approximated by a vertical straight line, $v = \theta$, but rather by a threshold equation of the form

$$u = g(v) \quad (1)$$

where one piece of the g curve is well fitted by the middle branch of the v nullcline. At hyperpolarized v values, the threshold curve is flat (Fig. 1C, E, F) or shows a hump (Fig. 1A, B). For a type I model (Fig. 1E, F), i.e., presenting a saddle point, the stable manifold of the sad-

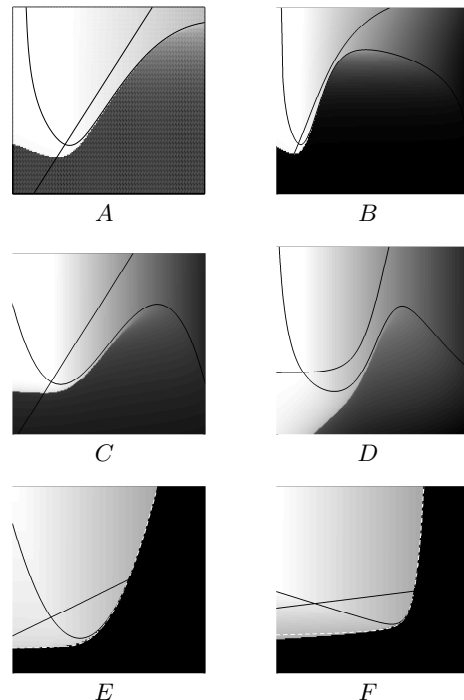


FIG. 1. Voltage response of bidimensional neural models. The gray level of a pixel indicates the maximum value reached by the membrane potential when the initial state of the neuron is where that pixel is located in the phase plane (v, u) (white is for low-voltage values and black is for high-voltage values). The corresponding voltage response is shown for (A) the 2D Abbott-Kepler reduction, (B) the Krinsky-Kokoz reduction, (C) the FitzHugh-Nagumo model, (D) the Morris-Lecar model, (E) the adaptive QIF and (F) the adaptive EIF. The nullclines are plotted (solid lines) together with the stable manifold of the saddle point (dashed lines) for the two last models (almost indistinguishable from the black region boundary).

dle point achieves a good approximation of the threshold manifold, corroborating previous results on the characterization of neural excitability. A reasonable choice for the threshold curve (1) is the sigmoidal curve defined by the Boltzmann function

$$g(v) = \frac{a}{1 + e^{-\lambda(v-\theta)}} + b \quad (2)$$

where b acts, at low v values, as a threshold on the recovery variable, θ determines the locus of the transition of the sigmoidal function, and λ gives the stiffness of the transition. A strict voltage threshold is retrieved in the limit $\lambda \rightarrow \infty$. To capture the fold that may occur near the resting state, a combination of two sigmoidal curves may be used. In this case, the function g in (1) is not invertible, and it is not possible to derive a threshold equation of the form $v = h(u)$. To assess the validity of the concept of threshold curve and to estimate the quality of its approximation by Boltzmann functions (2), an

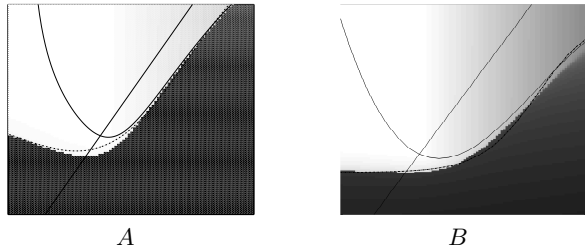


FIG. 2. Enlargement of the voltage response of (A) the 2D Abbott-Kepler reduction and (B) the FitzHugh-Nagumo model together with the corresponding threshold-curve approximation with (B) one or (A) two Boltzmann functions. The approximation closely matches the boundary between the spike region (in black) and the small voltage-response region (almost white). As in Fig. 1, the nullclines are shown.

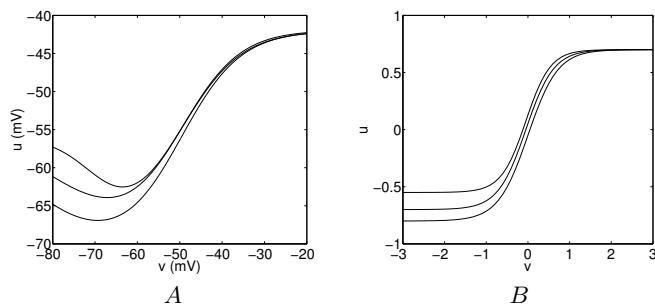


FIG. 3. Influence of the DC current on the threshold curve for (A) the 2D Abbott-Kepler model and (B) the FitzHugh-Nagumo model. From the bottom up, we used (A) $I = 0, 2, 4 \mu\text{A}/\text{cm}^2$ and (B) $I = 0, 0.1, 0.2$.

enlargement of the voltage response in a relevant area is displayed in Fig. 2 for the Abbott-Kepler reduction and the FitzHugh-Nagumo model.

To investigate the dependence of the threshold curve on the applied constant input current (DC current), we extract the threshold curve of the bidimensional Abbott-Kepler model (Fig. 3A) and of the FitzHugh-Nagumo model (Fig. 3B) for different input values. As can be seen, the injected DC current does not affect significantly the threshold curve except at hyperpolarized voltage values where a vertical shift of the threshold curve, i.e., along the u -axis, is observed. In addition, the sensitivity to inhibitory input can be enhanced due to a more pronounced hump as the DC current increased (Fig. 3A). Two-dimensional reductions of detailed neural models rely on the separation of time scales where it is commonly assumed that the fast dynamics, typically the sodium activation, is instantaneous. However, the sodium activation dynamics has an impact on the voltage trajectory of the neuron, and the main discrepancy between the original model and its reduction arises from the assumption

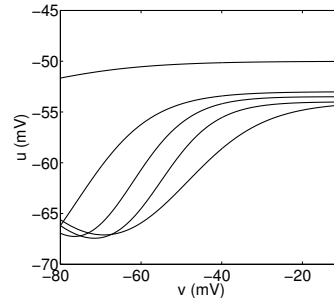


FIG. 4. Influence of the fast-sodium activation on the threshold curve. Projections of the threshold manifold of the three-dimensional Abbott-Kepler reduction in the (v, u) plane for different values of the sodium activation variable m , $m = 0.01, 0.1, 0.2, 0.3$ and 0.8 (from right to left).

that the fast time scale is instantaneous; i.e., the activation of sodium channels follows instantaneously the variation of the membrane potential [28]. To assess the impact of fast dynamics on the threshold curve, we consider the three-dimensional Abbott-Kepler reduction obtained by lumping together the slow variables of the Hodgkin-Huxley model and retaining the exact sodium activation dynamics [28]. We compute the threshold manifold in the three-dimensional state space, and we display in Fig. 4 five different projections (curves) on the (v, u) plane. We see that, as the sodium activation increased, the threshold curve is progressively shift to the left, i.e., the sensitivity to excitatory input is enhanced. This effect may be accounted for using $\theta \leftarrow \theta + \mu m$ in (2) where m is the sodium activation variable and $\mu > 0$ measures the sensitivity of the threshold surface to the sodium channel dynamics.

III. GENERALIZATION AND CONSEQUENCES

Let $x = (v, u_1, \dots, u_n)$ be the vector describing the neural activity where v is the membrane potential and $0 < u_i < 1$ are the activation or inactivation variables of ionic channels. Spikes are generated whenever a threshold condition is fulfilled that can be written in a general and abstract setting as $G(x)(t) = 0$ where G is a functional taking the trajectory $x(s)$, $s \leq t$ as an input; the excitability threshold at time t depends on the past history of the neuron state variables. Integrate-and-fire models assume the simplest form of threshold function where $G(x) = v - \theta$; the firing of a spike is determined comparing the membrane potential at the present time to a given fixed value. Based on the observations in the previous section, we define the following threshold equation:

$$g(v(t)) = \sum_{i=1}^n \alpha_i u_i(t) \quad (3)$$

where the weights α_i are constants whose sign determines its influence on the threshold: a negative weight facilitates excitation whereas a positive weight decreases the neural excitability, i.e., the effective voltage threshold is shifted to the right (at depolarized voltage values). In the following, we discuss the consequences of the threshold equation (3) on both neural dynamics and neural modeling.

A. Adapting Threshold

Let us consider the threshold hyperplane given by

$$v(t) = \theta_0 + \sum_{i=1}^n \alpha_i u_i(t) \quad (4)$$

obtained from (3) using the threshold function $g(v) = v - \theta_0$, which can be seen as a natural generalization of the strict voltage criterion used in standard integrate-and-fire models. Let us assume that each voltage-gated variable u_i follows the v -dependent first-order kinetics

$$\tau_i(v) \dot{u}_i = u_{\infty,i}(v) - u_i,$$

for $i = 1, \dots, n$, where in the subthreshold regime both functions $\tau_i(v)$ and $u_{\infty,i}(v)$ are assumed to be nearly constant and, in the super-threshold regime, the dynamics of u_i is reduced to an instantaneous change $u_i \leftarrow u_i + d_i$, i.e., ion channels rapidly open (or close) at high voltage values (or equivalently $\tau_i(v) \ll 1$ during a spike). Such spike-induced currents are traditionally used to describe adaptation or refractoriness.

Let t_k be the successive firing times of the neuron. The relaxation dynamics of u_i between firing events combined with the jump condition at firing times lead to

$$u_i(t) = u_{\infty,i} + \sum_k h_i(t - t_k), \quad (5)$$

where

$$h_i(t) = d_i \exp(-t/\tau_i) H(t),$$

with H is the Heaviside-step function. Using (5), the threshold hyperplane equation (4) can be rewritten as a dynamic voltage threshold $v(t) = \theta(t)$ where $\theta(t)$ is the time-dependent threshold given by

$$\theta(t) = \sum_k h(t - t_k) + \tilde{\theta}_0, \quad (6)$$

where

$$h(t) = \sum_{i=1}^n \alpha_i h_i(t),$$

$$\tilde{\theta}_0 = \theta_0 + \sum_{i=1}^n \alpha_i u_{\infty,i}.$$

We recover here the multi-timescale adaptive threshold (MAT) model introduced in [29] as a generalization of

the standard adapting threshold model.

The MAT model is therefore a specific instance of threshold hyperplane models where the number of threshold time constants is given by the number of voltage-gated variables playing a role in the threshold hyperplane, the different time scales of the MAT model are given by the time constants of the gating variables, and the weights associated with the time constants are given by the size of the jump of the related activation (or inactivation) variables (when the neuron assumes a spike) multiplied by their weights in the threshold hyperplane equation. From [29], it is expected that a threshold hyperplane with two ionic currents, and thus having two distinct time constants, is sufficient to achieve very good predictive performances. For identical ionic time constants, i.e., $\forall i \tau_i = \tau$, the threshold hyperplane is equivalent to the dynamic threshold

$$\tau \frac{d\theta}{dt} = \tilde{\theta}_0 - \theta, \quad (7)$$

with the instantaneous jump $\theta \leftarrow \theta + \sum_i \alpha_i d_i$ each time a spike is generated.

B. Dependence of the Voltage Threshold Upon the Subthreshold Activity

The threshold curve, Eq. (3), induces a dependence of the voltage threshold upon the subthreshold activity. This is illustrated in Fig. 5 where the 2D Abbott-Kepler reduction is stimulated by the subthreshold current

$$I_{syn} = g_{exc}(v - E_{exc}) + g_{inh}(v - E_{inh})$$

mimicking the stochastic arrival of excitatory and inhibitory presynaptic action potentials, modeled by homogeneous Poisson processes. Parameter g_{exc} (g_{inh}) is the excitatory (inhibitory) conductance consisting of the summed input from excitatory (inhibitory) synapses. Parameters E_{exc} and E_{inh} are the corresponding reversal potentials. The voltage trace is compared with the voltage threshold extracted from the threshold curve of the Abbott-Kepler model (see Fig 1A). The U shape of the threshold curve implies the existence of two voltage thresholds: an excitatory threshold that is reached for sufficiently strong excitation and an ‘‘inhibitory’’ threshold that is reached for hyperpolarizing current. Both thresholds show fluctuations that are correlated to the subthreshold voltage trajectory. When inhibition is blocked (at time $t = 100ms$, Fig. 5) a spike is emitted as predicted by the crossing of the excitatory threshold. After the spike, there is a short period where both thresholds are not defined producing a natural refractory period.

Most of voltage-dependent threshold models are, in fact, spike-dependent where the threshold trajectory is updated whenever a spike is emitted and subsequently decays toward a resting value (as illustrated in sec. III A). However, it has been observed for quite some time that

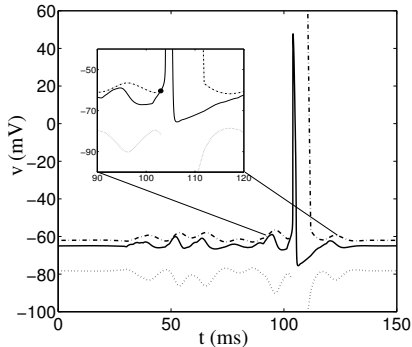


FIG. 5. Voltage trajectory of the 2D Abbott-Kepler model subject to conductance injection. The neuron is driven by an excitatory-inhibitory balanced input that maintains the membrane voltage between the two fluctuating voltage thresholds shown in the dot-dashed line (upper) and in the dotted line (lower). At time $t = 100\text{ms}$ the inhibition is blocked and a spike is elicited. The inset shows a zoom of the region where the excitatory threshold is reached.

the threshold also depends on the subthreshold activity, and, remarkably, well before the precise knowledge of neuronal ionic channels, Hill [30] proposed a dynamic threshold that rises with the subthreshold voltage. A threshold that depends on the voltage trajectory, and not only on the spike events, produces a rich phenomenology [31] and has been recently used to model post-inhibitory facilitation (PIF) [32, 33] and type III excitability [34]. We show here (see Appendix A) that such dynamical threshold models can be derived from bidimensional integrate-and-fire models with a threshold line where the dynamics of the recovery variable determines the properties of the voltage threshold.

C. Dependence of the Voltage Threshold Upon the Input

An implicit dependence of the voltage threshold upon the input is generated by the threshold criterion (3). We illustrate here this property using the spike-response-model

$$v(t) = \eta(t - t_f) + \int_0^\infty \kappa(s)I(t - s)ds \quad (8)$$

where η describes the shape of the spike and κ the response to an incoming short pulse. The spike timing t_f is the time at which the membrane potential crosses the threshold that we define here as the threshold line

$$v(t) = \theta_0 + \alpha u(t) \quad (9)$$

where u is an auxiliary variable given by

$$\dot{u} = a(bv - u).$$

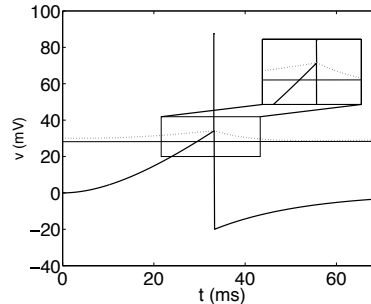


FIG. 6. Dependence of the threshold upon the input. Stimulation of the spike-response-model with a slow ramp input current. When the membrane potential reaches the threshold (dotted lines), a spike is emitted. The thin horizontal straight line indicates the spike threshold obtained from a brief current pulse.

Parameter $a > 0$ determines the time scale of u , and bv describes the influence of the voltage subthreshold fluctuations on u .

Integrating the u -dynamics, the threshold condition can be rewritten as

$$v(t) - \alpha ab \int_0^t v(s)e^{\alpha(s-t)} ds = \theta_0, \quad (10)$$

that depends on the voltage trajectory between spikes. A non-zero initial value of u will translate into a shift for θ_0 in (10): if at time $t = 0$ variable $u(t)$ is reset to u_r , the effective threshold becomes $\tilde{\theta}_0 = \theta_0 + \alpha u_r$. In Fig. 6 a slow ramp input is injected to the SRM model (8) with the threshold condition (10). As can be seen, the measured voltage for spike initiation is greater than the one obtained from a short current pulse (horizontal straight line).

Due to the strict voltage criterion commonly used in SRM-type models, the threshold difference between a slow ramp current and a short current pulse can not be reproduced. This limitation is overcome using the threshold line (9) where parameter $\alpha > 0$ mimics the influence of K^+ activation or Na^+ inactivation on the spike threshold. A negative α value accounts for spike facilitation.

D. Voltage Threshold Variability

We simulate the 2D Abbott-Kepler model with a super-threshold current and indicate in Fig. 7 the voltage values at which the threshold curve is crossed. In contrast with strict voltage threshold models, the threshold curve reproduces the small fluctuations of the critical voltage for spike initiation.

The variations of the voltage threshold depend on the input current making the prediction of spike timings with

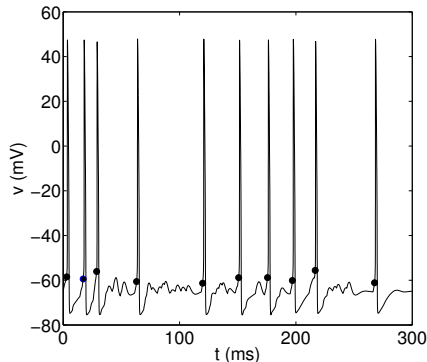


FIG. 7. Simulation of the 2D Abbott-Kepler reduction with fluctuating conductances. Black dots indicate the voltage value at which the threshold curve is reached. As predicted, a spike is initiated when the threshold condition is fulfilled.

fixed voltage threshold models uncertain and very sensitive to the firing value [4, 6]. In fact, the predictive quality of pure voltage threshold models severely degrades for small amplitude fluctuations of the input current due to a poor approximation of the effective threshold. One expects that the use of a threshold curve overcomes the issue of threshold fitting and provides a simple framework to improve the accuracy of simple predictive models.

E. Model Reduction and After-Spike Resetting

To avoid the simulation of the peak and the downstroke of an action potential, threshold rules are desirable to stop the simulation when a spike is initiated and to restart the integration after the spike duration. Therefore, in addition to the threshold criterion, one has to determine a restarting time together with initial values for state variables. Due to the low variability of spike duration, a fixed refractory period is commonly used. This period is followed by an update of the state variables that may be a “hard” after-spike reset $x \leftarrow x_r$ or an additive process $x \leftarrow x + d$. The former is mainly used to describe the after-spike update of the membrane potential, whereas the latter is commonly used for the recovery variable to account for adaptation. The resulting models belong to the class of integrate-and-fire models.

We propose here an integrate-and-fire approximation of the 2D Abbott-Kepler model where the threshold curve is defined as a combination of two sigmoidal functions. The duration of a spike is assessed using different initial conditions on the threshold curve, and the update rule is fitted by a hard reset for both variables. Parameter values of the reduced IF model are given in Appendix B. To assess the quality of the approximated IF model, we compare the trajectory of the original model with the one of the reduced model, both driven by the same fluctuat-

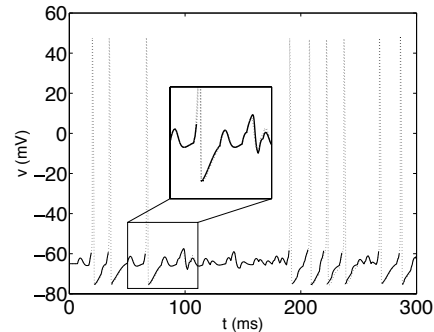


FIG. 8. Simulation of the 2D Abbott-Kepler model (dotted lines) and the corresponding integrate-and-fire approximation (solid line).

ing current. As shown in Fig. 8, the spike timings are correctly predicted by the threshold curve. In addition the subthreshold voltage trajectory is reproduced with a very high precision (trajectories are almost indistinguishable) indicating that both a constant spike duration and a hard reset for the two variables accurately capture the behavior of the original model. Note that the simulation restarts immediately after the sharp downstroke of the action potential, i.e., the spike afterpotential is simulated by the IF approximation.

F. Piecewise Approximation of Neural Models

A simple and numerically efficient approach to capture the threshold curves of spiking neurons is to use an idealized piecewise linear U curve made of two distinct parts, located in the hyperpolarized and depolarized region, called, respectively, the left branch and right branch hereafter. More precisely, the threshold curve is split into two pieces, defined by $x \cdot n_e = 0$ and $x \cdot n_i = 0$, that approximate the right and left branches of the threshold curve, respectively (see Fig. 9), where x is the state vector $x = (v, u)$ (for convenience, the origin is shifted to the turning point of the threshold curve), $n_e = (-\sin \theta_e, \cos \theta_e)$, and $n_i = (\sin \theta_i, \cos \theta_i)$. Angles θ_e and θ_i monitor the threshold location: θ_i is related to the hyperpolarized spike threshold (or “inhibitory” threshold), and θ_e measures the degree of excitability with respect to excitation. For $\theta_i = 0$, the left part of threshold curve is flat, and inhibitory inputs can not elicit spikes. When $\theta_e = \pi/2$, we recover a pure voltage threshold materialized by a vertical straight line in the phase plane. Depending on the branch of the threshold curve that is reached during the activity, different spike shapes (including different spike latencies) and different after-spike rules may be used. In particular, the spike latency observed in the 2D Abbott-Kepler model after a brief inhibitory input (simulations not shown) can be accounted

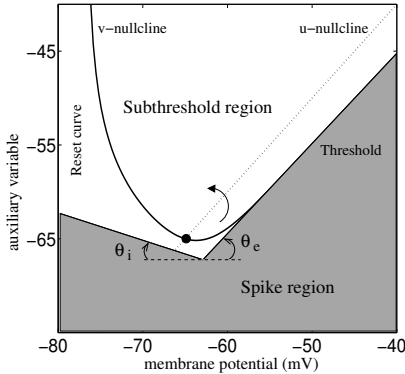


FIG. 9. Piecewise linear threshold for bidimensional spiking neuron. When the spike region is reached, i.e., the threshold curve is crossed, the trajectory restarts from the reset curve ($v = -80mV$).

for in its integrate-and-fire reduction adding a given pre-calculated latency.

Similarly to the piecewise-linear threshold, the nonlinear spike-generating currents of bidimensional spiking models may also be approximated by piecewise-linear functions defining a new class of IF models that are computationally cheap, amenable to event-driven simulations and analytically tractable. In addition, they are endowed with properties associated with fluctuating voltage thresholds.

When the dynamics of the membrane potential is mainly driven by the membrane voltage, i.e., u provides a negligible feedback on v , the auxiliary variable plays a role only in the definition of the threshold curve and the model can be further reduced to a one dimensional differential equation where the influence of the auxiliary variable is directly incorporated in the threshold criterion (see Eq. 10) where the convolution with the exponential kernel is responsible for a dependence of the threshold on the past to recent activity of the neuron.

G. Post-inhibitory Spikes, Accomodation and Facilitation

The two distinct branches of the U-shaped threshold curve are responsible for different dynamical features. The left part of the threshold curve, mainly located at hyperpolarized voltage values, induces post-inhibitory spikes: a strong enough brief inhibition pushes the trajectory leftward and drives the phase point across the hyperpolarized threshold evoking a rebound spike. Hyperpolarization-induced activity has been already reported in different models. Voltage-dependent dynamic threshold can exhibit spikes induced by fast inhibition [31, 33]. A modified type I FitzHugh-Nagumo model may fire at hyperpolarized states [35]. These post-inhibitory

spikes are closely related to the fold of the threshold curve near the rest state resulting in a second excitation threshold at hyperpolarized membrane potential. It is worth noting that this property differs from the well known phenomenon of anodal break excitation (or post inhibitory rebound) where a neuron fires after being released from a prolonged inhibition [36, 37].

The right branch of the threshold curve generates the so-called phenomenon of accomodation [30]: the critical voltage value for spike initiation obtained from slowly increasing input current is greater than the one derived from a very short current (see Sec. III C). The rise of the voltage threshold is monitored by the time constant of the recovery variable entering in the definition of threshold line and poorly depends on the membrane voltage equation. As v depolarizes, the auxiliary variable grows and the effective voltage threshold becomes larger. Therefore, spikes occur preferentially when the negative feedback does not operate on the threshold, i.e., when the rise of the voltage is sufficiently fast compared to the auxiliary variable dynamics. Such a mechanism amplifies coincident inputs [38].

An additional consequence of the excitatory threshold curve is the PIF phenomenon [32]: a subthreshold inhibitory event occurring in a favorable time window can facilitate spiking in response to a subsequent subthreshold excitation. The slope of the right branch of the threshold curve determines the degree of facilitation whereas the *window of opportunity* is controlled by the time constants of the model. The hyperexcitability period occurring in a time window preceding a subthreshold inhibitory input may result in a successful IE (inhibitory-excitatory) pair, and, by a symmetric and similar mechanism, a successful EI pair may be obtained. In fact, due to the U-shape of the threshold curve, post-excitatory facilitation (PEF) may occur in symmetry to the PIF effect: a subthreshold inhibition may elicit a spike if a preceding excitation is applied in a favorable time-window. However, the PEF phenomenon is less pronounced due to the attenuation of the left part of the threshold curve compared to its right part.

Interestingly these different features may be obtained independently of the nature of the rest state (node or focus, i.e., resonant or not [37]). In particular, it is not necessary to have an overshoot of the membrane voltage to observe post-inhibitory spikes or PIF. It is therefore possible to design an integrate-and-fire model of purely integrator type that exhibits post-inhibitory facilitation and may therefore prefer a certain resonant frequency. However, such a resonant behavior may be enhanced when the neuron acts, near the rest state, as a damped oscillator [37].

The dynamical properties generated by the two branches of the threshold curve may interplay. A resonant response associated with the left branch of the threshold curve (responsible for postinhibitory spikes) may interfere with resonant properties related to the right branch (responsible for postexcitatory spikes) leading to a com-

plex sensitivity to inhibitory-excitatory inputs. Moreover, it is well known that a brief inhibition can suppress the neural response to a super-threshold excitatory input. Conversely, a brief excitation can also cancel a post-inhibitory spike and excitation can therefore reduce the firing rate induced by inhibition [33]. Finally, PIF and PEF can occur simultaneously, resulting in output spikes evoked by combinations of subthreshold inhibitory and/or subthreshold excitatory events (that would be below threshold when delivered alone). This challenges the classical view of the role of inhibition in shaping the processing of spike trains [39].

IV. DISCUSSION

Due to its stereotyped nature, almost independent of the input, and its weak role in neural processing, the super-threshold regime of neural models is commonly reduced to a formal event, the so-called spike event. In this view, hybrid dynamical systems (HDSs) naturally arise [40, 41] to model the smooth excitable behavior of subthreshold integration combined with an after-spike update of the state variables (referred to as the jump transition map in the HDS terminology) when a threshold criterion (also defined as the autonomous jump set) is fulfilled. The subthreshold properties of neural HDSs have been largely discussed, and we place here our attention on the threshold equation, the so-called switching manifold in control sciences.

In this paper, we analyze the threshold manifold of bidimensional spiking neural models and show that the commonly used voltage equation $v = \theta$ poorly approximates the switching manifold of neural models. We suggest here a threshold criterion of the form $u = g(v)$ (which is preferable to $v = h(u)$; i.e., g may be non invertible) and show that such a threshold curve accounts for numerous features of spiking neurons traditionally associated with dynamical voltage threshold models. However, in contrast to conventional dynamical threshold models, the voltage threshold, defined by the threshold curve, may depend on subthreshold voltage fluctuations, and not only on spiking activity.

Depending on the dynamics of the auxiliary variable entering in the definition of the threshold criterion, different properties can be observed. For subthreshold-activated ionic channels (low-threshold currents), the associated threshold curve leads to a dependence of the voltage threshold upon the subthreshold activity and plays a significant role in post-inhibitory facilitation, type III excitability, and adaptation. Dynamical voltage thresholds that depend on the spiking activity can be derived from a threshold curve model where the auxiliary variable accounts for spike-triggered currents. In this framework, the time constants and the stationary value of the voltage threshold are directly related to the associated ionic channels.

Different modeling perspectives are offered by the con-

cept of threshold manifold. For instance, a simple one-variable leaky integrate-and-fire model can show hyperexcitability provided that the threshold equation incorporates a voltage-gated feedback. Features that are intuitively associated with resonate-and-fire models can also exist in integrator type models, as post-inhibitory spikes, as post-inhibitory facilitation, or as sensitivity to doublets.

A non-monotone threshold curve implies the existence of two voltage thresholds at both hyperpolarized and depolarized voltage values, challenging the common view of the role of inhibition in reducing excitability by pushing the system far from its spike threshold. This gives a more subtle concept of nearness to threshold than the one traditionally believed.

Appendix A: Integrate-and-Fire Neurons with a Threshold Line to Model Post-inhibitory Facilitation and Type III Excitability.

Let us consider the 2D integrate-and-fire model

$$\begin{aligned} \frac{dv}{dt} &= -v - \epsilon u + i_0 - i_{syn}, \\ \frac{du}{dt} &= \frac{u_\infty(v) - u}{\tau_u(v)} \end{aligned} \quad (\text{A1})$$

where a spike is emitted when the threshold line $v - u = \theta_0$ is crossed. Variable u provides a negative feedback on v whose strength is determined by $\epsilon > 0$. Let us assume that the corresponding ionic current has little effect on the subthreshold dynamics of $v(t)$, i.e., $\epsilon \ll 1$. Therefore u acts on the dynamics only through the threshold criterion. We further assume that (i) the relaxation time τ_u is almost constant during the subthreshold regime and (ii) the equilibrium function, $u_\infty(v)$, is given by the sigmoidal function

$$u_\infty(v) = \frac{u_a}{1 + e^{-\lambda(v-v_a)}}. \quad (\text{A2})$$

For small λ values the steady state function (A2) can be approximated by:

$$u_\infty(v) \approx \frac{u_a}{2} \left(1 + \frac{\lambda}{2} v - \frac{\lambda}{2} v_a \right).$$

Let us define $\theta(t) = \theta_0 + u(t)$, $\alpha = u_a \lambda / 4$, $\tilde{\theta}_0 = u_a / 2 - \alpha v_a + \theta_0$, and $\tau_\theta = \tau_u$. Model (A1) can be rewritten as the idealized PIF model introduced in [32]:

$$\begin{aligned} \frac{dv}{dt} &= -v + i_0 - i_{syn}, \\ \tau_\theta \frac{d\theta}{dt} &= \alpha v - (\theta - \tilde{\theta}_0) \end{aligned}$$

with the voltage threshold condition $v(t) = \theta(t)$.

Similarly, the nonlinear threshold dynamics $\tau_\theta d\theta/dt = \alpha + e^{b(v-c)} - \theta$ used to describe type III excitability [34]

can be recast as the nonlinear integrate-and-fire model (A1) where the equilibrium function (A2) is now approximated by

$$u_{\infty}(v) \approx u_a e^{\lambda(v-v_a)}$$

which is obtained from (A2) for v_a -values larger than sub-threshold voltage values, i.e., in the limit $e^{\lambda(v-v_a)} \ll 1$. In type III excitable neuron, the time scale of the voltage threshold (which is the time scale of the negative feedback, $u(t)$) is comparable to the neuronal time constant enabling a competition between the voltage rise and the negative feedback, and precluding spiking if the rise of the membrane voltage is too slow.

Appendix B: Integrate-and-fire Approximation of the 2D Abbott-Kepler Model.

The threshold curve, $u = g(v)$, of the 2D Abbott-Kepler reduction is approximated by a linear combination of two Boltzmann functions where parameters are determined using a least square method. We find

$$g(v) = -71 + \frac{23.2}{1 + e^{-0.18(v+54.4)}} + \frac{6.53}{1 + e^{-0.24(v+72.2)}}.$$

To estimate the spike duration and to derive the update rules, we use several initial conditions on the threshold curve. Two cases occur depending on the threshold crossing location. When the left part of the threshold curve is crossed, the spike shape shows different latencies, i.e., a delayed spike initiation is observed. The other part shows a poor variability and a spike duration of around 2ms is observed. In all cases, the after spike update is well approximated by a hard reset for the membrane potential, $v_r = -76mV$, and for the recovery variable, $u_r = -46mV$.

-
- [1] J. Rinzel, Fed. Proc. **44**, 2944 (1985).
- [2] J. Rinzel and B. Ermentrout, "Analysis of neural excitability and oscillations," in *Methods in Neuronal Modeling: From Synapses to Networks*, edited by C. Koch and I. Segev (MIT Press, Cambridge, MA, USA, 1998) Chap. 7, pp. 251–291, 2nd ed.
- [3] R. FitzHugh, Bull. Math. Biophysics **17**, 257 (1955).
- [4] W. M. Kistler, W. Gerstner, and J. L. van Hemmen, Neural Comput. **9**, 1015 (1997).
- [5] W. Gerstner and W. Kistler, *Spiking Neuron Models: Single Neurons, Populations, Plasticity* (Cambridge university press, 2002).
- [6] R. Jolivet, A. Rauch, H. R. Lüscher, and W. Gerstner, J. Comput. Neurosci. **21**, 35 (2006).
- [7] J. Platkiewicz and R. Brette, PLoS Comput. Biol. **6** (2010), 10.1371/journal.pcbi.1000850.
- [8] M. Desroches, M. Krupa, and S. Rodrigues, J. Math. Biol. **67**, 989 (2013).
- [9] J. Mitry, M. McCarthy, N. Kopell, and M. Wechselberger, Journal of Mathematical Neuroscience **3** (2013), 10.1186/2190-8567-3-12.
- [10] V. B. Kazantsev, A. T. Nguetcho, S. Jacquir, S. Binczak, and J. Bilbault, Neurocomputing **83**, 205 (2012).
- [11] J. P. Pfister, T. Toyoizumi, D. Barber, and W. Gerstner, Neural Comput. **18**, 1318 (2006).
- [12] R. Höpfner and K. Brodda, J. Math. Biol. **52**, 439 (2006).
- [13] Z. Piwkowska, M. Pospischil, R. Brette, J. Sliwa, M. Rudolph-Lilith, T. Bal, and A. Destexhe, J. Neurosci. Meth. **169**, 302 (2008).
- [14] P. Jahn, R. W. Berg, J. Hounsgaard, and S. Ditlevsen, J. Comput. Neurosci. **31**, 563 (2011).
- [15] S. Ditlevsen and P. Greenwood, J. Math. Biol. **67**, 239 (2013).
- [16] The threshold condition may be written as $v \geq \theta$. Since there is no ambiguity here on the meaning of the threshold, we write the threshold condition as an equality.
- [17] E. Izhikevich, *Dynamical Systems in Neuroscience: The Geometry of Excitability and Bursting* (MIT Press, 2007).
- [18] R. FitzHugh, J. Gen. Physiol. **43**, 867 (1960).
- [19] L. F. Abbott and T. B. Kepler, Lect. Notes in Phys. **368**, 5 (1990).
- [20] T. B. Kepler, L. F. Abbott, and E. Marder, Biol. Cybern. **66**, 381 (1992).
- [21] V. I. Krinsky and Y. M. Kokoz, Biofizika **18**, 506 (1973).
- [22] R. FitzHugh, Biophys. J. **1**, 445 (1961).
- [23] J. S. Nagumo, S. Arimoto, and S. Yoshizawa, Proc. IRE **50**, 2061 (1962).
- [24] C. Morris and H. Lecar, Biophys. J. **35**, 193 (1981).
- [25] E. Izhikevich, IEEE Trans. Neural Networks **14**, 1569 (2003).
- [26] N. Fourcaud-Trocmé, D. Hansel, C. van Vreeswijk, and N. Brunel, J. Neurosci. **23**, 11628 (2003).
- [27] R. Brette and W. Gerstner, J. Neurophysiol. **94**, 3637 (2005).
- [28] C. Meunier, Biol. Cyber. **67**, 461 (1992).
- [29] R. Kobayashi, Y. Tsubo, and S. Shinomoto, Front. Comput. Neurosci. **3** (2009), 10.3389/neuro.10.009.2009.
- [30] A. V. Hill, Proc. R. Soc. Lond. B **119**, 305 (1936).
- [31] S. Mihalas and E. Niebur, Neural Comput. **21**, 704 (2009).
- [32] R. Dodla, G. Svirskis, and J. Rinzel, J. Neurophysiol. **95**, 2664 (2006).
- [33] R. Dodla and J. Rinzel, Phys. Rev. E **73**, 010903 (2006).
- [34] X. Meng, G. Huguet, and J. Rinzel, Discrete Contin. Dyn. Syst. Ser. A **32**, 2729 (2012).
- [35] V. B. Kazantsev, Phys. Rev. E **64**, 056210 (2001).
- [36] R. FitzHugh, Biophys. J. **16**, 209 (1976).
- [37] E. Izhikevich, Neural Networks **14**, 883 (2001).
- [38] R. Azouz and C. M. Gray, Proc. Natl. Acad. Sci. USA **97**, 8110 (2000).
- [39] W. K. Luk and K. Aihara, Biol. Cybern. **82**, 455 (2000).

- [40] A. Tonnelier and W. Gerstner, Phys. Rev. E **67**, 021908 (2003).
- [41] E. Izhikevich, Phil. Trans. R. Soc. A **368**, 5061 (2010).